comments. Thanks are expressed to Eleanor Stagg for typewritting and to Jane Jorgensen for the drawings.

Appendix

All calculations were performed by using the extended Hückel method.[14] The orbital parameters along with the H_{ij} values are summarized in Table I. The bond lengths and angles for the osmium compounds were taken from ref 7, 11, and 15. For CpCo(NO)₂, the following structural data were used: Co–Cp-(center) = 1.72 Å; Co–N = 1.72 Å; N–O = 1.25 Å; ∠NCoN = 90°. For ethylene bonded to CpCo(NO)₂, the data are taken from ref 28.

Site Preferences and Bond Length Differences in CaAl₂Si₂-Type Zintl Compounds

Chong Zheng,[†] Roald Hoffmann,*[†] Reinhard Nesper,[‡] and Hans-Georg von Schnering*[‡]

Contribution from the Department of Chemistry and Materials Science Center, Cornell University, Ithaca, New York 14853, and Max-Planck-Institut für Festkörperforschung, D-7000 Stuttgart 80, FRG. Received September 16, 1985

Abstract: The Al₂Si₂²⁻ two-dimensional networks in the CaAl₂Si₂ structure may be derived by a conceptual splitting of the wurtzite lattice and a subsequent reconstruction. The reconstruction suggests some analogies with organic propellanes. The resulting Al₂Si₂²⁻ network has two four-coordinate sites, a normal tetrahedral one, and another with a highly distorted local umbrella geometry. A choice is made by Al and Si for one or the other of these sites, a choice whose causes we explore in detail. We begin with a comparison of the energetics of the normal and the "inverted" phase, based on the dispersion of the bands. To avoid destabilizing high dispersion in the filled bands, the more electronegative atoms should occupy the less "dispersive" positions in the crystal. We also examine the Si–Al bonds of the SiAl₄ "inverted" tetrahedron as isolated from and incorporated into the CaAl₂Si₂ lattice. When an isolated SiAl₄⁸⁺ model is flipped from T_d to C_{3v} geometry, the 1-fold Si–Al bond is weakened more than the 3-fold bond. The reasons for this bring us again close to an organic propellane model. When the SiAl₄ motif is incorporated into the lattice, additional inter-unit-cell interaction enhances the difference between the two types of Si–Al bonds. The possibility of an alternative "dimerized graphite"-type structure is also explored.

Zintl's concept[1] plays an important role in solid-state chemists' thinking and in their understanding of a large range of crystal structures. In this simple but extremely powerful concept, the electropositive elements are thought of merely as electron donors, donating electrons to the conjoined more electronegative element bonding partners. The latter then comply with the octet rule by receiving those electrons. An example is the NaTl structure,[2] **1**, in which Na donates one electron to Tl, and the Tl⁻ moieties, isoelectronic to Pb, therefore similar to C, form the diamond structure. The Na⁺ cations build another diamond lattice, in-

zinc-blende structure, and the Li⁺ ions sit in the center of the tetrahedra formed by the Si atoms.

O Li   ⊘ Al   ● Si

2 LiAlSi

Though simple and most useful, Zintl's rule is not a universal predictor of molecular structure. It does not give us any hint as to why NaAlSi[4] is not isostructural with LiAlSi or how the bond length should change when going from one structure to another. More sophisticated theoretical calculations are needed to explain

○ Na   ● Tl

1 NaTl

terpenetrating the Tl⁻ one. Closely related to the NaTl structure is the LiAlSi phase,[3] **2**. Here the (AlSi)⁻ network forms a

†Cornell University.
‡Max-Planck-Institut für Festkörperforschung.

(1) See: Klemm, W. *Proc. Chem. Soc., London* **1958**, 329; Schäfer, H.; Eisenmann, B.; Müller, W. *Angew. Chem., Int. Ed. Engl.* **1973**, *12*, 694.
(2) Zintl, E.; Dullenkopf, W. *Z. Phys. Chem.* **1932**, *B16*, 195–205.
(3) (a) Schuster, H.-U.; Hinterkeuser, H.-W.; Schäfer, W.; Will, G. *Z. Naturforsch., B* **1965**, *31B*, 1540–1541. (b) Christensen, N. E. *Phys. Rev. B* **1985**, *32*, 6490.
(4) Westerhaus, W.; Schuster, H.-U. *Z. Naturforsch.* **1979**, *34B*, 352–353.

the structural details of these Zintl phases. These can be provided but at the cost of obliteration of the powerful simplicity of the original concept.

In this contribution, we discuss one important AB_2X_2 structural type, the $CaAl_2Si_2$ structure.[5] The structure is easily understood as a Zintl phase; at the same time, a detailed orbital analysis of this popular structural type reveals interesting details of the bonding.

The $CaAl_2Si_2$ structure is shown in **3**. Two-dimensional rafts of Ca^{2+} ions are separated by tightly bound $Al_2Si_2^{2-}$ layers. These

$\bigcirc$ Ca O Al $\bullet$ Si
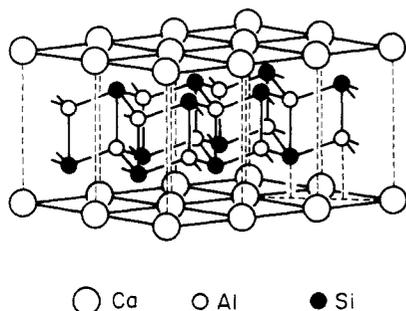
3 CaAl₂Si₂

layers can in turn be described (and that is all it is for the moment, a description) as being made up from two stacked AlSi layers, each such layer being a two-dimensional infinite net of chairlike six-membered rings.

Each atom in the Al_2Si_2 layer is four-coordinate, but the coordination environment is very different for Al and Si. The local coordination sphere is shown schematically in **4**. Each Al is

4

surrounded approximately tetrahedrally by four Si atoms. The Si is also four-coordinate in Al, but the environment is most unusual, a flipped tetrahedron or umbrella shape. This is untypical for Si, but it is what one approaches and attains in a class of most interesting strained organic molecules called "propellanes", **5a**, or their isolobal[7a] analogue **5b**.[7b]

5

There is another instructive way to view this structure. Many solid-state phases can be viewed from the point of view of discrete cluster groupings and their progressive condensation.[8] Still other structures may be conveniently imagined as "split" from three-dimensional Zintl networks.[9] The $CaAl_2Si_2$ structure is such. $Al_2Si_2^{2-}$ or $AlSi^-$ is isoelectronic to AlN, so one is led to think of the wurtzite lattice. This can be cleaved by "intercalating" Ca^{2+} layers, as shown in **6**. The splitting and intercalation prevent

$\bigcirc$ Ca O Al $\bullet$ Si
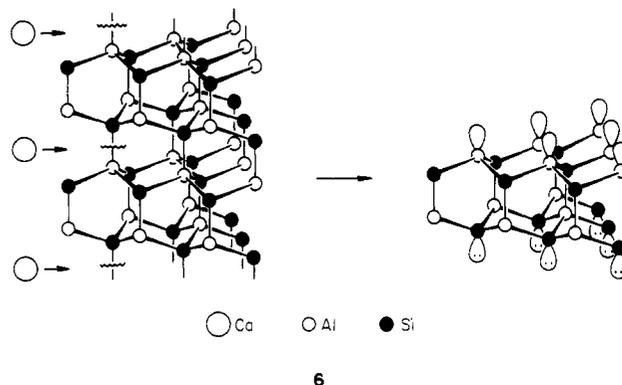
6

vertical bonding between hexagonal $Al_2Si_2^{2-}$ layers. Dangling bonds result which will seek for bonding partners. This is what happens on a clean Si surface[10]—a reconstruction—and one way to view the $CaAl_2Si_2$ structure is in a similar way, as indicated in **7** → **8**.
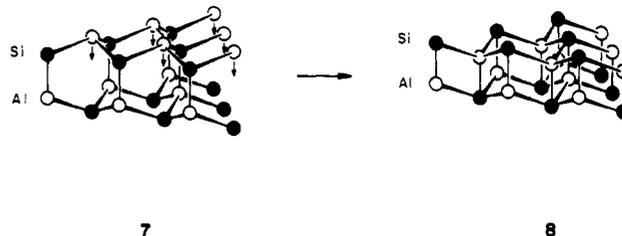
7   **8**

This way of thinking provides us with a connection between a three-dimensional structure and a two-dimensional lattice. At the moment, this is a paper exercise, but it may be more than that; a line of development in solid-state chemistry is the tailoring of three-dimensional solids into lower dimensional ones and modifying the interfaces between lower dimensional layers to produce desired physical properties.[11]

Given the "splitting out + reconstruction" viewpoint, an obvious question is that of site preference: why is it that the reconstruction is such that the Al atoms become tetrahedral and Si atoms find themselves in the umbrella geometry (**7** → **8**) and not the reverse (**9** → **10**). We proceed to examine this question, as we do others arising in this paper, with band calculations of the extended Hückel type. Details of the computations are given in the Appendix.

Site Preferences in the $Al_2Si_2^{2-}$ Layer of $CaAl_2Si_2$. It is useful to examine first the geometrical constraints of the alternative structures. In **8**, the Al reside at the center of Si_4 tetrahedra, which

(5) Gladyshevskii, E. I.; Kipyakevich, P. I.; Bodak, O. I. *Ukr. Fiz. Zh.* (*Russ. Ed.*) **1967**, *12*, 447–453.

(6) (a) Ginsburg, D. "Propellanes"; Verlag-Chemie: Weinheim, 1975. (b) Greenberg, A.; Liebman, J. F. "Strained Organic Molecules"; Academic Press: New York, 1978. The [1.1.1]propellane was first synthesized in Wiberg's group. (c) Wiberg, K. B.; Walker, F. H. *J. Am. Chem. Soc.* **1982**, *104*, 5239–5240. (d) Michl, J.; Radziszewski, G. J.; Downing, J. W.; Wiberg, K. B.; Walker, F. H.; Miller, R. D.; Kovacic, P.; Jawdosiuk, M.; Bonačić-Koutecký, V. *Pure Appl. Chem.* **1983**, *55*, 315–321. And there have been many theoretical studies on propellanes. Here is a selection of references on these: (e) Newton, M. D.; Shulman, J. M. *J. Am. Chem. Soc.* **1972**, *94*, 773. (f) Stohrer, W.-D.; Hoffmann, R. *J. Am. Chem. Soc.* **1972**, *94*, 779. (g) Dodziuk, H. *J. Compt. Chem.* **1984**, *5*, 571–575 and references cited therein. (h) Vučković, D. Lj.; Vujisić, Lj. *Croat. Chem. Acta* **1984**, *57*, 801–810 and references cited therein. (i) Wiberg, K. B. *J. Am. Chem. Soc.* **1983**, *105*, 1227. (j) Wiberg, K. B.; Dailey, W. P.; Walker, F. H.; Waddell, S. T.; Crocker, L. S.; Newton, M., unpublished results, personal communication.

(7) (a) Hoffmann, R. *Angew. Chem.* **1982**, *94*, 725; *Angew. Chem., Intl. Ed. Engl.* **1982**, *21*, 711. (b) Andrianov, V. G.; Struchkov, Yu. T.; Kolobova, N. E.; Antonova, A. B.; Obezyuk, N. S. *J. Organomet. Chem.* **1976**, *122*, C33–C36.

(8) (a) Corbett, J. D. *Pure Appl. Chem.* **1984**, *56*, 1527–1543. (b) Simon, A. *Angew. Chem.* **1981**, *93*, 23–44, *Angew. Chem., Int. Ed. Engl.* **1981**, *20*, 1–22. (c) von Schnering, H. G. *Angew. Chem.* **1981**, *93*, 44–63, *Angew. Chem., Int. Ed. Engl.* **1981**, *20*, 33–51.

(9) Some researchers have identified some clusters with a portion of bulk metals or minerals, for example: $[Pt_{38}(CO)_{44}]^{2-}$ with Pt fcc metal: (a) Chini, P. *J. Organomet. Chem.* **1980**, *200*, 37. $[Co_8S_6(SPh)_8]^{4-}$ with pentlandite, Co_9S_8: (b) Christou, G.; Hagen, K. S.; Holm, R. H. *J. Am. Chem. Soc.* **1982**, *104*, 1744. It is also possible to produce clusters by quenching the vapor from the crystal in He gas or by cutting crystals via ion bombardment. (c) Martin, T. P. *Ber. Bunsenges. Phys. Chem.* **1984**, *88*, 300–301.

(10) (a) Kahn, A. *Surf. Sci. Rep.* **1983**, *3*, 193–300. (b) Pauling, L.; Herman, Z. S. *Phys. Rev. B* **1983**, *28*, 6154–6156.

(11) Rao, C. N. R.; Thomas, J. M. *Acc. Chem. Res.* **1985**, *18*, 113.

9

10
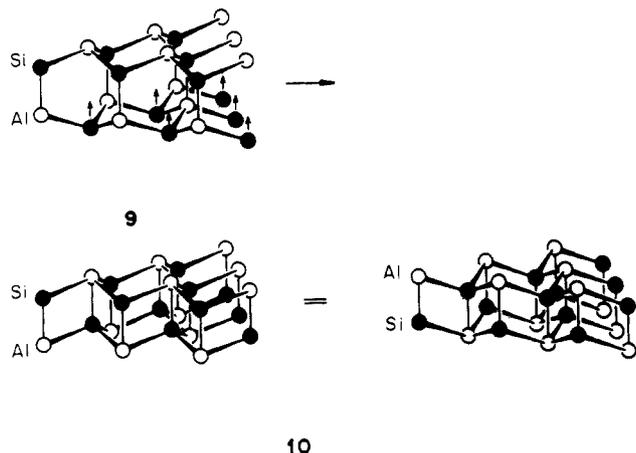
then pack together (**11**) to form the layer. For an ideal tetrahedral

11
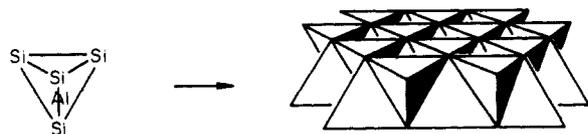
arrangement, the Si⋯Si contact is $2^{1/2}$ times as long as the Al⋯Al separation, as shown in **12a**. In the layer derived from **9** → **10**, the situation is reversed, **12b**.
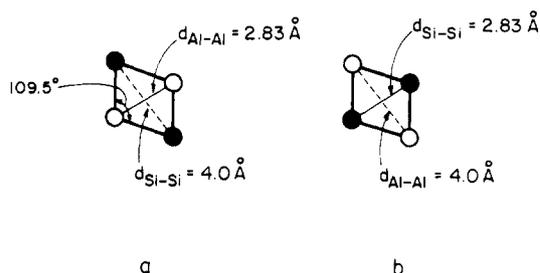
12

Imagine the $Al_2Si_2^{2-}$ layer built up from Al–Si⁻ dinuclear monomers, emphasized by the bold lines in **13**. The schematic interaction diagram for the diatomic is shown in Figure 1. When

13
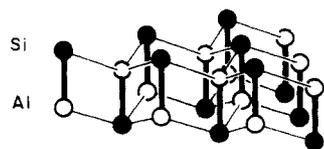
the more electronegative Si interacts with Al, its orbitals are pushed down, resulting in four low-lying orbitals in the dinuclear unit which are mainly descendants of the one s and three p orbitals of Si. The eight valence electrons of the AlSi⁻ unit reside in these four Al–Si bonding orbitals, with an energy gap between the four low-lying orbitals and another four high-lying orbitals, mainly of Al character, and Al–Si antibonding.

On to the solid state: When these AlSi⁻ units are arranged in the $Al_2Si_2^{2-}$ layer as in **13**, the shorter Al⋯Al contact indicated in **12a** should result in a greater dispersion of those bands concentrated on Al. These constitute the upper block of the AlSi⁻ orbitals in Figure 1. In contrast, the occupied lower block of the AiSi⁻ diatomic unit should generate bands of lesser width, due to the larger separation between the Si atoms in the $Al_2Si_2^{2-}$ layer.
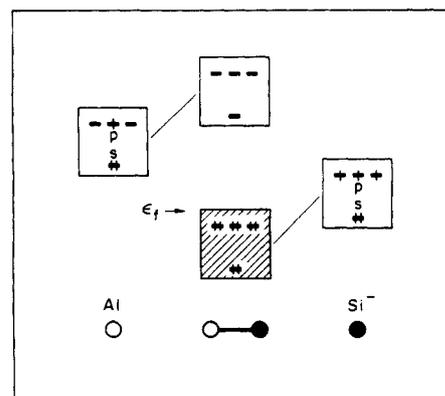
Figure 1. Schematic interaction diagram of Al and Si⁻ to form Al–Si⁻.
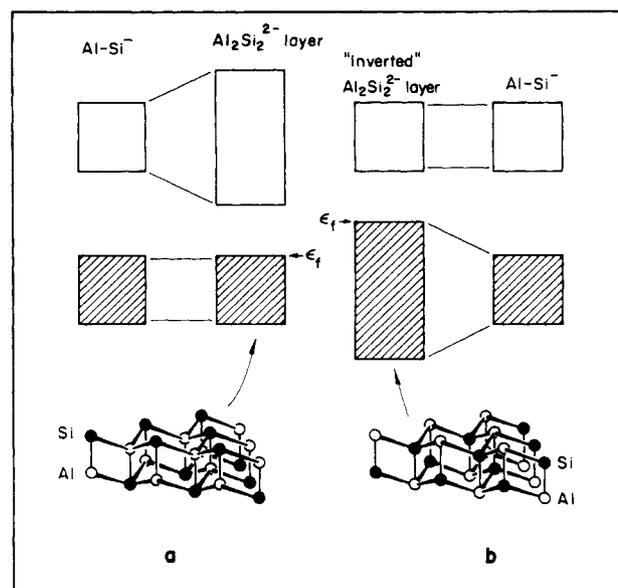
Figure 2. Schematic picture showing the difference in the filled and unfilled band dispersion between the normal, a, and the inverted, b, $Al_2Si_2^{2-}$ layers.
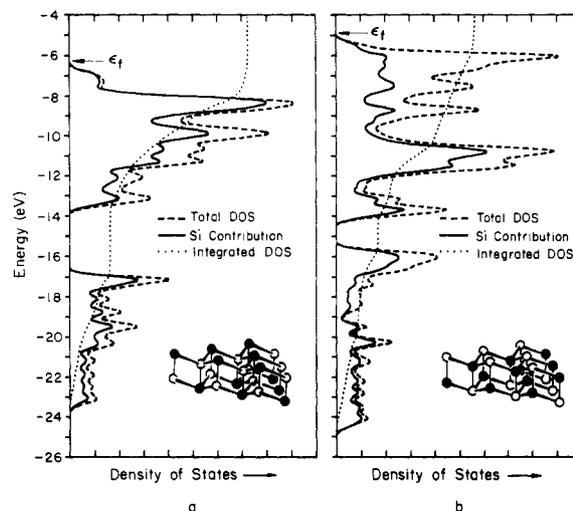
Figure 3. Density of states (dashed lines) and the Si contribution to it (solid lines) of the normal, a, and the inverted, b, $Al_2Si_2^{2-}$ layers. The dotted lines are integrated Si states, indicating that more than 70% of the Si states is filled in the normal $Al_2Si_2^{2-}$ layer, a, but less than 60% of the Si states is below the Fermi level in the inverted one, b.

The situation is shown schematically in Figure 2a.

The inverted layer, **10**, will have the greater dispersion in the lower, occupied, mainly Si block bands (Figure 2b). This is a consequence of the coupling overlap being mainly Si⋯Si, the

CaAl₂Si₂-Type Zintl Compounds

J. Am. Chem. Soc., Vol. 108, No. 8, 1986 1879
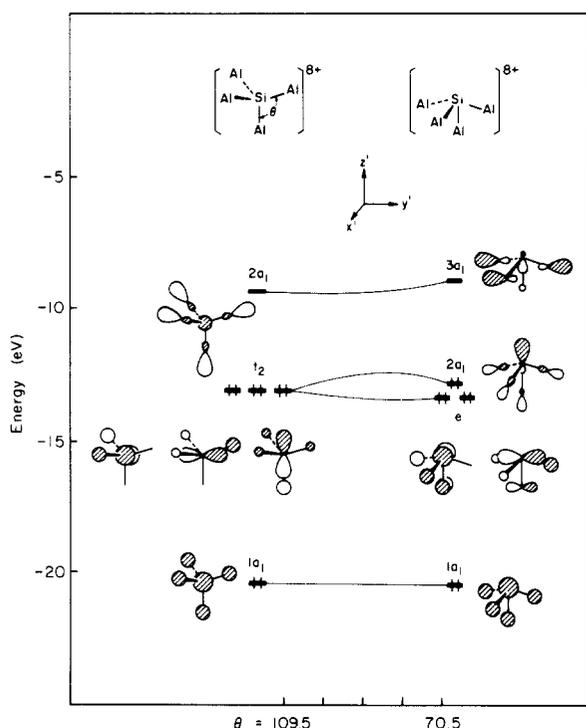
Figure 4. Walsh diagram for the "flipping" process of the $SiAl_4^{8+}$ species from T_d to C_{3v} geometry.
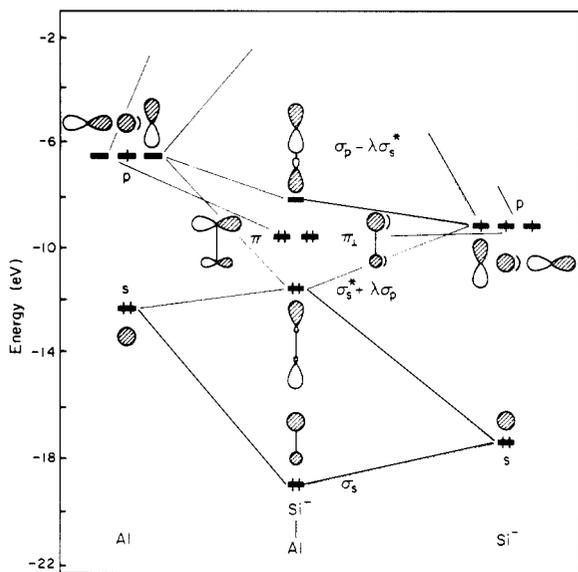
Figure 5. Interaction diagram for Al–Si⁻ formed from Al and Si⁻.

Figure 6. MO diagram for the $Al_2Si_2^{2-}$ motif as isolated from the $Al_2Si_2^{2-}$ lattice.

shortest inter-unit distance (**12b**).

The situation becomes clear now: the bigger dispersion in the completely filled lower block in the inverted $Al_2Si_2^{2-}$ layer in Figure 2b is the solid-state equivalent of a filled shell or four-electron repulsion.[12] The result is a higher Fermi energy and a destabilization relative to the normal $Al_2Si_2^{2-}$ structure, **8**.

The specific rationalization of the observed site preference in CaAl₂Si₂ is actually an example of a much broader conclusion: When a compound contains two nonequivalent lattice sites, one of which is more dispersive (shorter contact between the equivalent sites of that type) than the other, the more electropositive element should reside in the more dispersive site. This conclusion, which we will describe in some detail elsewhere,[13] depends on having a highly occupied band. When the lattice site preferences do not follow this rule but invert, as they sometimes do,[14] the phenomenon

becomes most interesting and merits further study.

We will discuss the band structure of CaAl₂Si₂ below, but let us anticipate the result by extracting some of the conclusions relative to the present discussion. Figure 3 shows the calculated density of states (DOS) for both layers **9** and **10**. The solid lines indicate the contribution of Si, states to the total DOS; what is left over under the dashed lines is to be assigned to Al. It is quite clear that in the inverted layer represented by Figure 3b, these mainly Si states have greater dispersion.

We should also mention here a significant point made by one of the reviewers: There may also be an electrostatic, Madelung energy contribution to the preference for net **8** over **10**. In **8**, the negative Si atoms are nearer to the Ca^{2+} sheets; in **10**, it would have been the relatively positive Al atoms.

Inequivalent Bonds at Si. On going from wurtzite to $Al_2Si_2^{2-}$, the aluminum environment remains tetrahedral, but the coordination geometry at Si changes drastically, from tetrahedral to "umbrella", as shown in **14**. There are two kinds of bonds, which

14

we will call "handle" (the unique axial one) and "rib" (three such). The experimental observation is that the handle bond is longer than the rib bond in all CaAl₂Si₂ compounds except some in which there is a transition metal at the Al position with a d⁵ configuration.[15] We will treat the transition-metal cases in a separate contribution.

(12) (a) Salem, L. *Chem. Br.* **1969**, *5*, 449. (b) Salem, L. *J. Am. Chem. Soc.* **1968**, *90*, 543.
(13) Zheng, C.; Hoffmann, R., unpublished results.

(14) Eisenmann, B.; May, N.; Müller, W.; Schäfer, H. *Z. Naturforsch., B* **1972**, *B27*, 1155–1157.
(15) (a) Cordier, G.; Schäfer, H. *Z. Naturforsch, B* **1976**, *B31*, 1459–1461.
(b) Mewis, A. *Z. Naturforsch, B* **1978**, *B33*, 606–609. (c) Brechtel, E.; Cordier, G.; Schäfer, H. *Z. Naturforsch, B* **1978**, *B33*, 820–822.

$$\frac{1}{\sqrt{3}} \quad + \quad \frac{1}{\sqrt{3}} \quad + \quad \frac{1}{\sqrt{3}} \quad = $$

$p_z \qquad\qquad p_y \qquad\qquad p_x \qquad\qquad\qquad p_{z'}$

16

$$\frac{1}{\sqrt{2}} \quad - \quad \frac{1}{\sqrt{2}} \quad = $$

$p_x \qquad\qquad p_y \qquad\qquad p_{x'}$

17

$$-\frac{2}{\sqrt{6}} \quad + \quad \frac{1}{\sqrt{6}} \quad + \quad \frac{1}{\sqrt{6}} \quad = $$

$p_z \qquad\qquad p_y \qquad\qquad p_x \qquad\qquad p_{y'}$

18
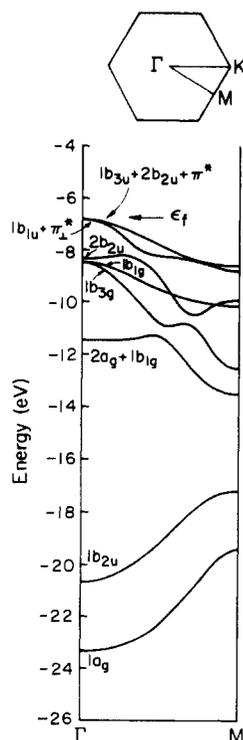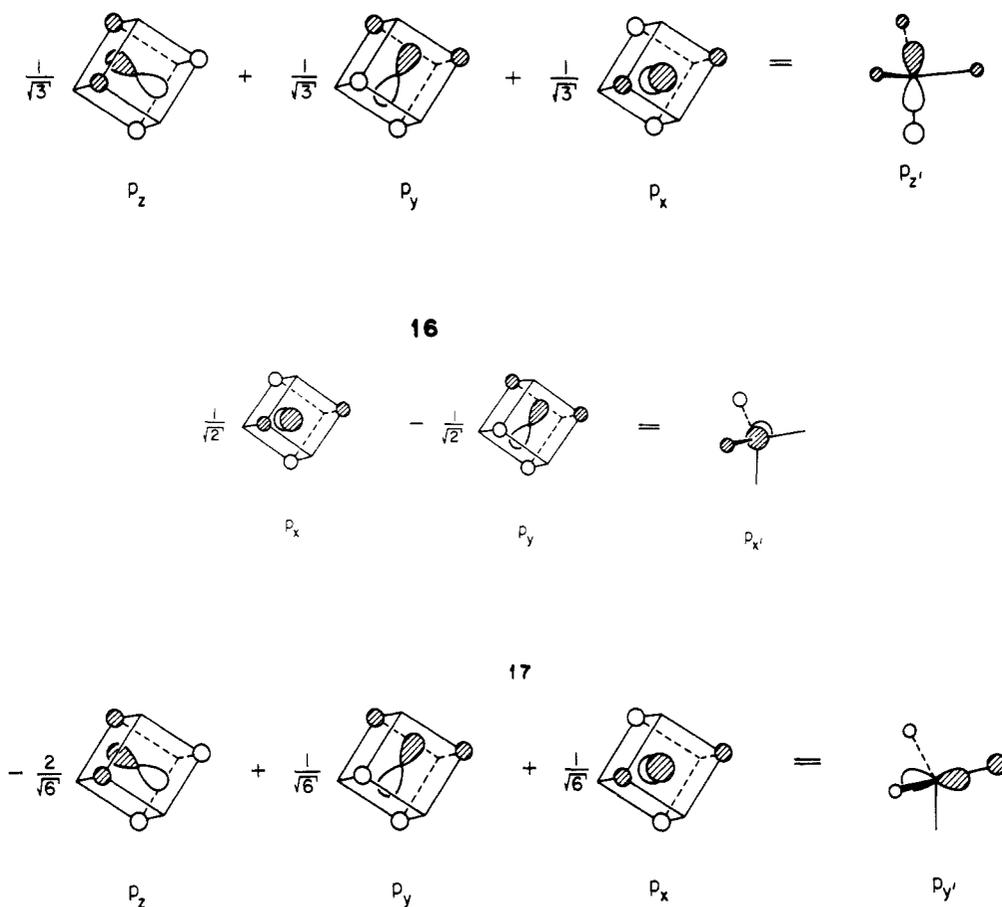
Figure 7. Band structures of the $Al_2Si_2^{2-}$ layer. Main contributions at the Γ point are indicated.

Table I lists a selection of main group element compounds in this structure type. The bond length difference between rib (1×)

and handle (3×) bonds is clearly seen.

Let us try to understand the origins of this bond length differential. Since the local environment changes in a significant way only around Si, let us model the solid-state process by an umbrella flipping in a cluster, $SiAl_4^{8+}$. Figure 4 is a Walsh diagram for this process. On the left-hand side of Figure 4, we see the levels of an undistorted $SiAl_4$ tetrahedron. The five orbitals shown are (in increasing energy) one a_1 orbital, a bonding combination of Si s and Al s orbitals; three degenerate t_2 orbitals, bonding combinations between Si p and Al, mainly, s orbitals; and one unfilled a_1 orbital, mainly a bonding combination between Si s and Al p orbitals.

The three degenerate t_2 orbitals are not drawn with the conventional[27] choice of linear combinations for the degenerate orbital (15). That choice is appropriate to a subsequent deformation

(16) Zheng, C.; Hoffmann, R., unpublished results.
(17) Deller, K.; Eisenmann, B. *Z. Naturforsch, B* **1977**, *B32*, 612–616.
(18) Klüfers, P.; Mewis, A. *Z. Naturforsch, B* **1977**, *B32*, 753–756.
(19) Mewis, A. *Z. Naturforsch, B* **1978**, *B33*, 382–384.
(20) Klüfers, P.; Mewis, A.; Schuster, H.-U. *Z. Kristallogr.* **1979**, *149*, 211–225.
(21) Brechtel, E.; Cordier, G.; Schäfer, H. *Z. Naturforsch., B* **1979**, *B34*, 921–925.
(22) Schuster, H.-U.; Fischer, H.-O. *Z. Naturforsch, B* **1979**, *B34*, 1169–1170.
(23) Mewis, A. **1980**, *B35*, 939–941.
(24) Fischer, H.-O.; Schuster, H.-U. *Z. Naturforsch., B* **1980**, *B35*, 1322–1323.
(25) Mahan, A.; Mewis, A. *Z. Naturforsch., B* **1983**, *B38*, 1041–1045.
(26) Nesper, R.; von Schnering, H. G.; Curda, J. *Z. Naturforsch., B* **1982**, *B37*, 1514–1517.
(27) (a) Cotton, F. A. "Chemical Applications of Group Theory", 2nd ed.; Wiley-Interscience: New York, 1971; p 228. (b) Gimarc, B. M. "Molecular Structure and Bonding"; Academic Press: New York, 1979; pp 50–51.

CaAl₂Si₂-Type Zintl Compounds

J. Am. Chem. Soc., Vol. 108, No. 8, 1986 1881
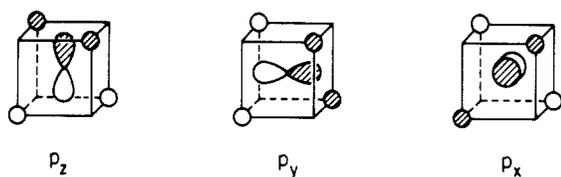
15

maintaining an S_4 axis, e.g., to D_{2d}. What we require here is preparation for a deformation which preserves a 3-fold axis, e.g., to C_{3v}. The appropriate combinations are **16**, **17**, and **18**. **16** is concentrated along one bond; **17** and **18** are perpendicular to that bond. If the symmetry is lowered to C_{3v}, **16** transforms as a_1 and **17** and **18** transform together as e.[28]

Now imagine starting the umbrella inversion process. t_2 splits into e + a_1, the a_1 combination being $p_{z'}$ in **16** and e being $p_{x'}$ and $p_{y'}$ in **17** and **18**. As the shape of the latter indicates, a change in the handle to the rib angle θ (see **14**) down from tetrahedral will not change the Si p–Al s overlap much. Thus, the e set is expected to remain more or less constant in energy with θ.

The a_1 $p_{z'}$ orbital will go up in energy, due to the antibonding that develops between the three Al s orbitals and the negative lobe of the Si $p_{z'}$ orbital, as shown in **19**. Of course, when the sym-

19

metry is lowered from T_d to C_{3v}, this orbital of a_1 symmetry will mix with other a_1 orbitals, in particular orbital $2a_1$ in Figure 4. This mixing, indicated in **20**, reduces the antibonding between the three Al s orbitals and the Si $p_{z'}$ orbital by hybridizing the $p_{z'}$ at the cost of severely weakening the "handle" (1×) Si–Al bond.

20

The resulting overlap populations are shown in **21**. Note the weaker handle bond. In fact, both types of bonds are weakened relative to the tetrahedron. This is consistent with the predom-

21

inant destabilization of $2a_1$ with θ (see Figure 4). However, when θ decreases from 109.5° to 70.5°, additional bonding is provided between the handle and the rib Al atoms. The extra stabilization

---

(28) Albright, T. A.; Burdett, J. K.; Whangbo, M.-H. "Orbital Interactions in Chemistry"; Wiley: New York, 1985; p 138.

Table I. Some AB_2X_2 Compounds assuming the $CaAl_2Si$ Structure

compound	bond length, Å		ref
	rib or 3× B–X	handle or 1× B–X	
CaAl₂Si₂	2.40	2.57	5
CaMg₂As₂	2.639	2.733	17
CaMg₂Sb₂	2.846	2.922	17
SrMg₂Sb₂	2.859	2.907	17
BaMg₂Sb₂	2.888	2.889	17
CaMg₂Bi₂	2.902	2.976	17
BaMg₂Bi₂	2.946	2.986	17
CaZn₂P₂	2.445	2.538	18
CaCd₂P₂	2.615	2.787	18
CaZn₂As₂	2.527	2.608	18
CaCd₂As₂	2.698	2.837	18
CaZn₂Sb₂	2.698	2.788	19
CaCd₂Sb₂	2.865	2.971	19
SrZn₂Sb₂	2.711	2.795	19
SrCd₂Sb₂	2.872	2.972	19
ThCu₂P₂	2.411	2.410	20
YbZn₂P₂	2.440	2.541	20
YbZnCuP₂	2.409	2.465	20
BaCd₂Sb₂	2.883	2.969	21
CeLi₂As₂	2.582	2.725	22
SrZn₂As₂	2.549	2.606	23
SrCd₂As₂	2.715	2.826	23
YbMnCuP₂	2.411	2.472	23
PrLi₂P₂	2.546	2.612	24
PrLi₂As₂	2.561	2.773	24
NdLi₂As₂	2.567	2.711	24
ZrCu₂P₂	2.315	2.409	25
YZnCuP₂	2.418	2.474	25
LaZnCuP₂	2.461	2.480	25
CeZnCuP₂	2.450	2.463	25
GdAl₂Si₂	2.503	2.537	26

operates through the e orbitals, in which the p orbitals of the handle Al point toward the rib Al's and result in good overlap between them. The overlap population in **21** confirms this observation. The energetic difference is very small, with the C_{3v} more stable than the T_d geometry by 2 kcal/mol in our calculation.

Wiberg and co-workers have performed ab initio calculations on the umbrella bending for methane.[29] For θ = 90°, the umbrella handle bond length (r_1 = 1.114 Å) is longer than the umbrella rib one (r_2 = 1.080 Å), in agreement with our $SiAl_4^{8+}$ expectations based on overlap populations.

On moving to the two-dimensional infinite slab, local molecular orbitals develop into bands. We have to speak not of individual levels but of densities of states. But the essential local features will be maintained in the extended solid. For example, the extended solid equivalent of the overlap population for the $Al_2Si_2^{2-}$ layer, the COOP curves,[30] which we will discuss later, will show that around the Fermi level (or HOMO), there is an antibonding feature in the vertical (1×) Si–Al bond and the overlap population for that bond is smaller than that of the rib (3×) Si–Al bond. This is exactly the same as in the discrete cluster $SiAl_4^{8+}$ case. We will see, however, that there are some novel features added in the extended material.

Band Structures. We will now build up the band structures from the molecules. In this $Al_2Si_2^{2-}$ layer, there are two Si–Al dinuclear units per unit cell, connected together as in **22a**. The repeating motif is **22b**. For an ideal tetrahedral arrangement in the $Al_2Si_2^{2-}$ layer, the bond length ratio $d_{Si-Al}/d_{Al-Al} = 3^{1/2}/2$, so the primary bonding between dinuclear units within one unit cell is Si–Al. The additional Al···Al interaction can be viewed as a perturbation.

Each SiAl⁻ has the typical orbitals of a heteronuclear diatomic (Figure 5). Each filled orbital is mostly on Si, one 3s and three

---

(29) (a) Wiberg, K. B.; Ellison, G. B.; Wendoloski, J. J. *J. Am. Chem. Soc.* **1976**, *98*, 1212. (b) Wiberg, K. B.; Ellison, G. B. *Tetrahedron* **1974**, *30*, 1573.

(30) Some other applications of the COOP curves may be found in: (a) Wijeyesekera, S. D.; Hoffmann, R. *Organometallics* **1984**, *3*, 949. (b) Kertesz, M.; Hoffmann, R. *J. Am. Chem. Soc.* **1984**, *106*, 3453. (c) Saillard, J.-Y.; Hoffmann, R. *J. Am. Chem. Soc.* **1984**, *106*, 2006.
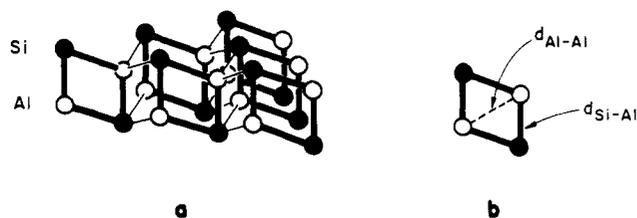
22

mostly 3p, with some Al admixture.

The eight filled orbitals of the repeating dimer $Si_2Al_2^{2-}$ (**22b**) are shown in Figure 6. Substantial second-order mixing changes the orbitals significantly from just being in- and out-of-phase combinations of the dinuclear monomer unit in Figure 5. The lowest orbital $1a_g$ is the in-phase combination of the lowest s orbitals of each unit. The out-of-phase combination, however, will build into the molecular orbital some antibonding character between the two Si–Al units. To alleviate this, the σ s orbitals will mix in some π character from the Si–Al π orbitals of higher energy, thus forming $1b_{2u}$. The counterpart of $1b_{2u}$ is $2a_g$, at higher energy. $1b_{3u}$ and $1b_{1g}$ are the descendants of Si–Al π orbitals, mixed to some extent with the Si–Al σ_p–$\lambda\sigma_s^*$ orbitals. $1b_{1u}$ and $1b_{3g}$ are derived from Si–Al $\pi_\perp$ orbitals (perpendicular to the plane of the paper).

When the $Al_2Si_2^{2-}$ lattice is constructed from the SiAlAlSi motif, **22b**, these MO's will develop into bands. For example, the $1a_g$ can be propagated into the lattice in either an in-phase way, corresponding to the Γ point in the Brillouin zone, **23**, or in an out-of-phase way, **24**, corresponding to the M point in the Brillouin zone. The in-phase propagation **23**, of course, stabilizes the crystal
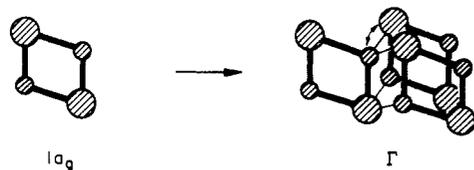
23
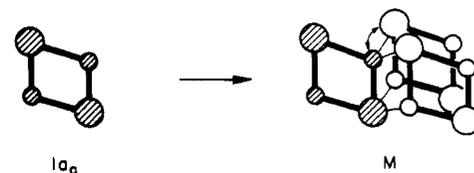
24

orbital by building up bonding character between the MO's of different unit cells, as indicated by the arrow in **23**. The out-of-phase propagation clearly destabilizes the crystal orbital, as also indicated by the arrow in **24**. So going from Γ to M, this band should rise in energy.

The behavior of each band as a function of k could be developed in a similar way. The actual band structure that results is plotted in Figure 7, for the line $\Gamma \rightarrow$ M. The main contributions to each band at the Γ point are specified in Figure 6.[31] As we have concluded above, the lowest band, mainly composed of the $1a_g$ orbital, goes up in energy from Γ to M. The other bands are not all in the same energy order as in Figure 6, a consequence of substantial inter-cell interaction and mixing between these orbitals. An example of what happens follows: If the $1b_{1u}$ orbital in Figure

---

(31) Orbitals of different symmetries of the $Al_2Si_2^{2-}$ motif (D_{2h}) can mix at the Γ point, because the Γ point has different symmetry.
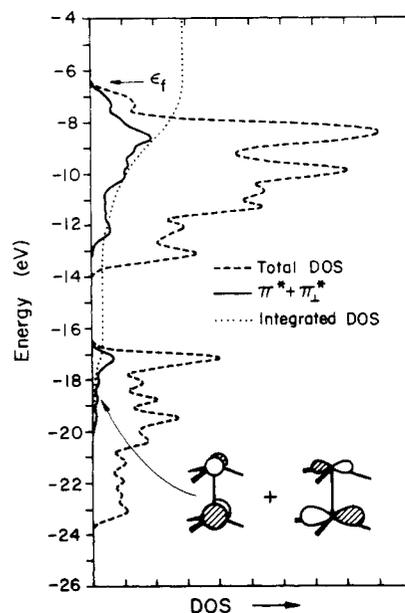
Figure 8. Density of states (dashed line) and the contribution to it from the π^* and $\pi_\perp^*$ orbitals of the Al–Si$^-$ monomer (solid line) in the $Al_2Si_2^{2-}$ layer. The dotted line is the integrated DOS of π^* and $\pi_\perp^*$ states, indicating that about 30% of them is filled.

6 were to propagate in an in-phase way, corresponding to the Γ point in the Brillouin zone, antibonding character would build up between the $1b_{1u}$ orbitals in adjacent unit cells, as shown in **25**.
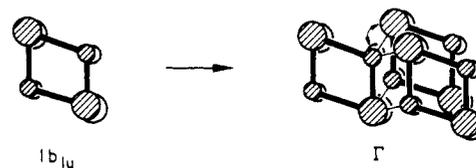
25

However, when another $2b_{1u}$ orbital of higher energy, the descendant of the Si–Al $\pi_\perp^*$ orbitals, is propagated throughout the lattice, it is bonding which is built up between unit cells, as shown in **26**. **25** and **26** will mix, maximizing inter-unit-cell bonding, at the cost of loss of intra-unit-cell vertical bonding.
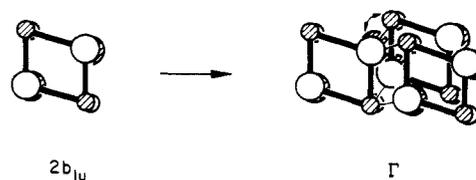
26

Figure 8 shows the contribution of the $\pi_\perp^*$ to the total DOS. As we can see, the mixing of this locally Al–Si antibonding level into occupied bands is substantial. π^* mixes into the occupied bands in a similar way. A consequence of this mixing in π^* and $\pi_\perp^*$ is some accumulation of Si–Al antibonding character (in the handle or vertical or 1× bond) around the Fermi level.

Figure 9 shows the COOP curves for the vertical (solid line) and the tilted (dotted line) Si–Al bonds. Indeed an antibonding bump is observed in the vertical Si–Al COOP, near the top of the p bands.

The computed overlap populations in the solid are shown in **27**, and these should be compared with the cluster model **21**. There is a reasonable correspondence between the extended solid
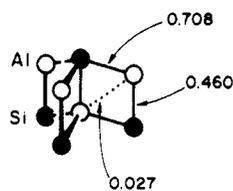
27

values (computed for equal Si–Al distances but reflected in the observed distance inequalities) and the cluster model for the solid.

There are several consequences of a weakened vertical bond and the specific way in which it is weakened. First of all, it is possible to intercalate small ions into this $Al_2Si_2^{2-}$ layer,[32] shown in **28** for $LnLi_3P_2$. This material can be thought of as $LnLi'Li_2P_2$ in which Li' intercalates into a $CaAl_2Si_2$-type $LnLi_2P_2$ structure. Other compounds of this type are $LnLiCu_2P_2$.[25]
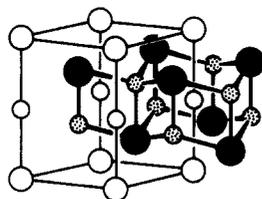
28

Note that Si–Al vertical antibonding character is concentrated near the top of the p band (Figure 9). Oxidation of the layer should then shorten the vertical Si–Al bond. There are some such compounds, with 15 electrons per unit cell.[33] However, no single crystal study is yet available for these. It would also be interesting to intercalate some valence fluctuator[34] ($Eu^{2+} \leftrightarrow Eu^{3+}$, for example) instead of Ca, the oxidation or reduction of which might affect the bonding in the host lattice. A compound, $GdAl_2Si_2$, with 17 electrons has been made.[26] The extra electron probably resides in the Gd d band, providing the observed metallic behavior, as indicated schematically in **29**.

29

(32) (a) Grund, I.; Schuster, H.-U. *Z. Anorg. Allg. Chem.* **1984**, *515*, 151–158. (b) Kuss, M.; Schuster, H.-U. *Z. Kristallogr.*, in press.

(33) Zwiener, G.; Neumann, H.; Schuster, H.-U. *Z. Naturforsch.*, *B* **1981**, *B36*, 1195–1197.

(34) "Valence Instabilities"; edited by Wachter, P., Boppart, H., Eds.; North-Holland: Amsterdam, 1982.
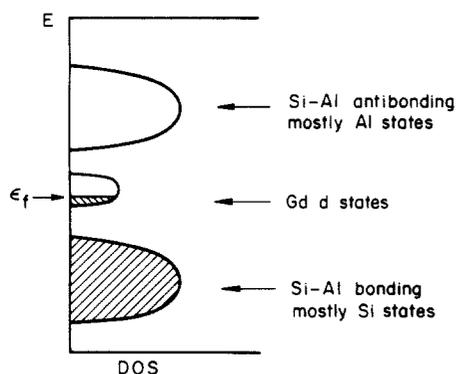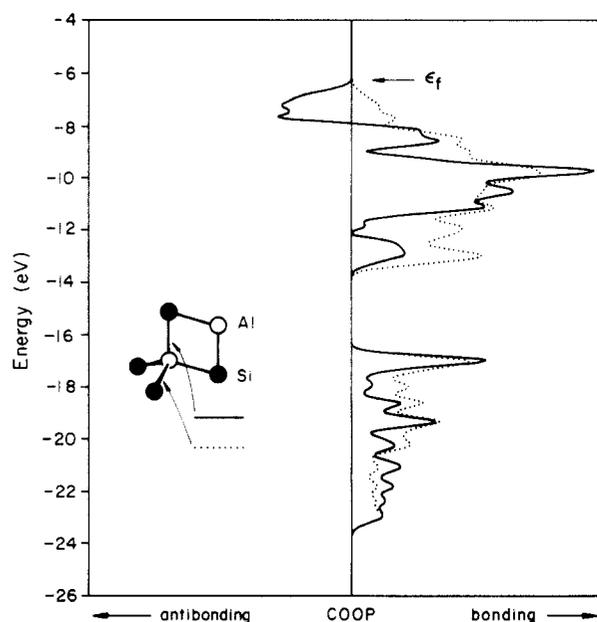
Figure 9. Crystal orbital overlap population curves for the 1-fold (solid line) and the 3-fold (dotted line) Si–Al bonds.

Table II. Extended Hückel Parameters

orbitals		H_{ii}, eV	ζ
Al	3s	−12.3	1.17
	3p	−6.5	1.17
Si	3s	−17.3	1.38
	3p	−9.2	1.38

Finally, the reconstruction process **7–8**, where the local environment change is shown in **30**, is not the only one. The other possibility is **31**, similar to the intramolecular recombination to
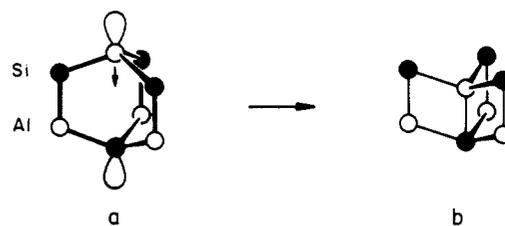
30

tricyclo[2.2.2.0]octane, i.e., [2.2.2]propellane of the bicyclic diradical. The resulting structure is of a "dimerized" graphite net type, **32**. Our calculation shows that the two structures **30b** and
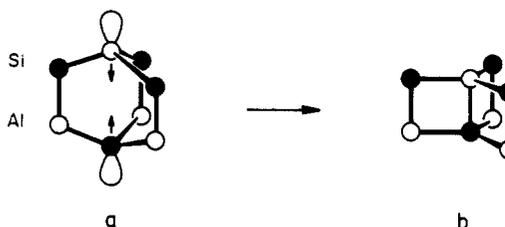
31

31b have approximately the same energies for $Al_2Si_2^{2-}$. However, the closer contact between Si atoms in **31b** results in a negative overlap population, shown in **33a**, compared to the structure **30b** whose overlap populations are depicted in **33b**. The negative overlap population in **33a** is due to the closed-shell repulsion

32

between Si atoms, formally Si^{4-}. However, when the electro-
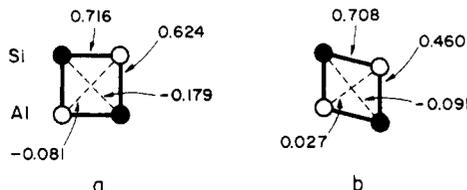
33

negativity difference between the B (open circle) and the X (black circle) atoms is decreased, the repulsion should be minimized. So a stoichiometry of $B_2'B_2''^-$ (or $X_2'X_2''^-$) should increase the pos-

sibility of the "dimerized" graphite structure **32**.

Appendix

The extended Hückel method[35] was used in all calculations. Table II lists the parameters used for Al and Si. The geometry is chosen such that Si is at the center of an idealized Al_4 tetrahedron with Si–Al = 2.45. A 30 k-point set is used in the irreducible wedge in the Brillouin zone[36] to calculate average properties.

(35) Hoffmann, R. *J. Chem. Phys.* **1963**, *39*, 1397; Hoffmann, R.; Lipscomb, W. N. *J. Chem. Phys.* **1962**, *36*, 2179, 3489; **1962**, *37*, 2872. Ammeter, J. H.; Bürgi, H.-B.; Thibeault, J. C.; Hoffmann, R. *J. Am. Chem. Soc.* **1978**, *100*, 3686.
(36) Pack, J. D.; Monkhorst, H. J. *Phys. Rev. B* **1977**, *16*, 1748.

Ligand Effects on the Electronic Structure, Spectra, and Electrochemistry of Tetracobalt Carbonyl Clusters

Gary F. Holland,[1a] **Donald E. Ellis,**[*1a] **and William C. Trogler**[*1b]

Contribution from the Department of Chemistry, Northwestern University, Evanston, Illinois 60201, and Department of Chemistry, D-006, University of California at San Diego, La Jolla, California 92093. Received August 21, 1985

Abstract: Self-consistent field Xα calculations using the discrete variational method (SCF–Xα–DV) have been performed for $Co_4(CO)_{12}$ (I) and the C_{3v} symmetry model clusters $(\eta\text{-}C_6H_6)Co_4(CO)_9$ (II), $Co_4(CO)_9[(PH_2)_3CH]$ (III), and $(\eta\text{-}C_6H_6)Co_4(CO)_6[(PH_2)_3CH]$ (IV) to explore the effect of phosphine and arene ligands on cluster electronic structures. Density of states plots have been used to simplify analysis of bonding trends in these complex clusters. The cluster core charge varies from 3.11, to 2.58, to 2.41, to 1.80 e along the I–IV series. Charge on the apical Co is least positive in the arene-capped cluster II while basal cobalts are least positive in IV. Ionization potential calculations support qualitative Hückel studies that suggested $(\eta\text{-}C_6H_6)M$ fragments bind more strongly to other metal centers than isolobal $M(CO)_3$ fragments. Electronic absorption spectra of I, $(\eta\text{-}MeC_6H_5)Co_4(CO)_9$ (V), $Co_4(CO)_9(\text{tripod})$ (VI) (tripod = $(PPh_2)_3CH$), $(\eta\text{-}MeC_6H_5)Co_4(CO)_6(\text{tripod})$ (VII), and $(\eta\text{-}C_6Me_6)Co_4(CO)_6(\text{tripod})$ (VIII) exhibit low-energy features between 1000 and 400 nm. Arene-capped clusters exhibit an extra low-energy absorption and calculations for the models II and IV assign this to a HOMO–LUMO transition that resembles intramolecular charge transfer from the apical to basal cobalt atoms. All substituted cobalt clusters V–IX (IX = $(\eta\text{-}[2.2]\text{-}$paracyclophane)Co_4(CO)_6(\text{tripod}))$ exhibit reversible 1e reductions by cyclic voltammetry. Only clusters VI and VII display reversible 1e oxidations. Redox potentials correlate well with calculated tetracobalt core charges for the model systems I–IV but do not correlate well with HOMO or LUMO energies. Effects of apical and basal substitutions on redox potentials in the tetracobalt clusters are shown to be additive. This supports the notion of delocalized cluster bonding. For this reason cluster core charges better reflect gross properties of the cluster rather than HOMO or LUMO energies of localized two-electron orbitals.

Electronic structures of dinuclear metal complexes have been thoroughly studied,[2] resulting in well-characterized one-dimensional metal–metal interactions. An understanding of the electronic structure of larger clusters,[3] beyond electron counting rules,[4]

has not yet been achieved. Trinuclear clusters, which exhibit two-dimensional metal–metal interactions, have been the most extensively studied class of large clusters. Calculations for triangular $M_3(CO)_{12}$ (M = Ru, Os) complexes using extended Hückel theory (EHT)[5] and the self-consistent field Xα discrete

(1) (a) Northwestern University. (b) University of California at San Diego.
(2) (a) Cotton, F. A.; Walton, R. A. "Multiple Bonds between Metal Atoms"; Wiley: New York, 1982. (b) Geoffroy, G. L.; Wrighton, M. S. "Organometallic Photochemistry"; Academic Press: New York, 1979. (c) Lever, A. B. P.; "Inorganic Electronic Spectroscopy"; Elsevier: Amsterdam; 1984.

(3) Manning, M. C.; Trogler, W. C. *Coord. Chem. Rev.* **1981**, *38*, 89–138.
(4) Wade, K. In "Transition Metal Clusters"; Johnson, B. F. G., Ed.; Wiley-Interscience: Chichester, 1980.
(5) (a) Korol'kov, D. V.; Miessner, H. Z. *Z. Phys. Chem. (Leipzig)* **1973**, *253*, 25–32. (b) Tyler, D. R.; Levenson, R. A.; Gray, H. B. *J. Am. Chem. Soc.* **1978**, *100*, 7888–7893.